Polyclonality of familial murine adenomas: Analyses of mouse chimeras with low tumor multiplicity suggest short-range interactions

Andrew T. Thliveris*†‡, Richard B. Halberg*‡, Linda Clipson*, William F. Dove*§¶, Ruth Sullivan‖, Mary Kay Washington, Stephen Stanhope††, and Michael A. Newton†††‡‡**

*McArdle Laboratory for Cancer Research, Departments of †Ophthalmology and Visual Sciences, ††Statistics, and ‡‡Biostatistics and Medical Informatics, §Laboratory of Genetics, and ‖Waisman Center, University of Wisconsin, Madison, WI 53706; and **Department of Pathology, Vanderbilt University Medical Center, Nashville, TN 37232

Contributed by William F. Dove, March 31, 2005

In previous studies demonstrating the polyclonal structure of familial intestinal adenomas, high tumor multiplicity made it difficult to eliminate the possibility that polyclonality arose by the random collision of distinct initiated clones as opposed to some form of clonal interaction. We sought to test further the random collision hypothesis. Chimeric mice carrying the multiple intestinal neoplasia (*Min*) mutation of the adenomatous polyposis coli gene (*Apc*) and homozygous for the tumor resistance allele of the *Mom1* locus were established. These chimeras also display a strong propensity for tumors of polyclonal structure, despite their markedly reduced tumor multiplicity. Considering tumor sizes and multiplicities, the observed fraction of overtly polyclonal heterotypic adenomas was significantly higher than predicted by the random collision hypothesis. This finding supports models of polyclonality involving interaction among multiple initiated clones. The extent of clonal interaction was assessed by statistical analyses that relate the observed frequency of overtly polyclonal heterotypic tumors to the geometry of the chimeric patches and the pattern of underlying crypts. These statistical calculations indicate that the familial adenomas of the $Apc^{Min/+}$ mouse may commonly form through interactions between clones as close as 1–2 crypt diameters apart.

Bayesian image reconstruction | clonal interactions | colon cancer | spatial statistics | tumorigenesis

Most current models of tumorigenesis involve a monoclonal origin. The evidence for monoclonality at the earliest stages of spontaneous intestinal neoplasia is limited. Intestinal adenomas and carcinomas in carcinogen-treated mice (1, 2) and large adenomas in humans (3) seem to be monoclonal. The clonality of normal and neoplastic tissue is assessed by the analysis of patches in chimeras or mosaics heterotypic for a clonal lineage marker. The ability to detect polyclonality in early human tumors is restricted by the large patch sizes of X-inactivation mosaics (4). The first indication that familial intestinal adenomas were commonly polyclonal in structure came from a study of a mosaic XY ↔ XO male patient with familial adenomatous polyposis (5). In that study, 5% of microadenomas were found to have a mixed karyotype, which led the authors to suggest that as many as 76% are polyclonal (ref. 5 but see ref. 6). Novelli *et al*. (5) suggested that primary adenoma formation involved cooperation between initiated cells or, alternatively, that the mixed karyotype arose by mosaicism within a clonal tumor through loss of the Y chromosome from subpopulations of neoplastic cells, owing to mitotic instability of the dicentric Y chromosome.

In a subsequent study using mice heterozygous for the multiple intestinal neoplasia (Min) allele of the adenomatous polyposis coli gene (*Apc*) and chimeric for the ubiquitously expressed lineage reporter gene *Gt*(*ROSA*)*26Sor*^{tm1Sor} (*ROSA26*) expressing lacZ, Merritt *et al*. (7) observed that 22 of 251 (9%) adenomas were overtly polyclonal by being heterotypic for the blue (ROSA26) and white (non-ROSA26) neoplastic lineages. Four hypotheses were entertained:

- Mosaicism within the adenoma by loss of the heterozygous *lacZ* marker: Unlike the dicentric Y chromosome involved in the XY ↔ XO study (5), the *lacZ* transgene shows no mosaicism in the C57BL/6 (B6) $Apc^{Min/+}$ mice carrying *ROSA26*/+, making this explanation implausible.
- Epigenetic silencing of lacZ expression: When heterotypic tumors were analyzed for the marker *D6Mit36* linked to the *lacZ* insertion, no white adenomatous regions were found that carried the 129/Sv allele linked to the *ROSA26-lacZ* marker.
- Random collision between independently arising neoplasms: The high tumor multiplicity in the chimeric mice of this study, and in the XY ↔ XO human with familial adenomatous polyposis studied by Novelli *et al*. (5), made this a possible explanation for the origin of polyclonal adenomas (see ref. 7).
- Polyclonality via active interaction between multiple initiated clones: Several variations of this model were favored by Merritt *et al*. (7) including interaction between crypts promoting somatic loss of heterozygosity at the *Apc* locus; interaction during the transition to dysplastic growth, as in the "community effect" for developmental transitions (8); and interaction between initiated clones favoring tumor survival or growth.

The evaluation of polyclonality in both the familial adenomatous polyposis patient analyzed by Novelli *et al.* (5) and the chimeric B6 Min mice (mice carrying $Apc^{Min/+}$) analyzed by Merritt *et al.* (7) was compromised by high tumor multiplicity. In the latter case, it was estimated that a model of passive clonal interaction could explain the overall frequency of heterotypic adenomas if the intestinal epithelium is heterogeneous with only a portion of the tissue susceptible to tumorigenesis. Regional heterogeneity could involve exposure to dietary carcinogens. Indeed, recent studies have found that adenomas in B6 Min mice form predominantly in the distal segment of the small intestine (9). We have therefore assessed the incidence of heterotypic tumors in chimeric Min mice in which the tumor multiplicity has been strongly reduced by homozygosity for the resistance allele of the *Mom1* modifier locus ($Mom1^R$).

In this analysis at low multiplicity, we have explicitly studied the chimeric patch size distribution in the neighborhood of tumors. A statistical analysis of these data indicates that random collision between independent neoplasms is a highly unlikely

Abbreviations: *Apc*, adenomatous polyposis coli gene; B6, C57BL/6; *Min*, multiple intestinal neoplasia; Min mice, mice carrying $Apc^{Min/+}$; *ROSA26*, *Gt*(*ROSA*)*26Sor*^{tm1Sor}.

‡A.T.T. and R.B.H. contributed equally to this work.

¶To whom correspondence should be addressed. E-mail: dove@oncology.wisc.edu.

explanation of the incidence of polyclonal adenomas in familial intestinal neoplasia. More likely, the early adenomas in Min mice involve an interaction among clones that lie as close as 1–2 crypt diameters apart.

Materials and Methods

Mouse Strains and Generation of Aggregation Chimeras. B6 Min mice were obtained from our colony that is maintained by continually backcrossing to B6/J mice (The Jackson Laboratory) imported every fifth generation. B6 mice heterozygous for the *ROSA26* transgene expressing LacZ were obtained from The Jackson Laboratory. B6 $Mom1^{R/R}$ mice were obtained from our congenic line that carries a $\approx 4 \times 10^6$-bp region from the resistant AKR strain lying between markers *D4Mit54* and *D4Mit13* on mouse chromosome 4 (10, 11). The $Mom1^R$ resistance region was made homozygous on the B6 Min and B6 *ROSA26*/+ backgrounds. Aggregation chimeras were generated by fusing embryos from two crosses: B6 $Apc^{+/+}$ $Mom1^{R/R}$ × B6 $Apc^{Min/+}$ $Mom1^{R/R}$ and B6 $Apc^{Min/+}$ $Mom1^{R/R}$ × B6 *ROSA26*/+ $Mom1^{R/R}$.

Offspring were screened for *Min* and the *ROSA26* transgene, using PCR assays of DNA isolated from toe clips. Ear snips were also taken from each animal and stained with X-Gal to ascertain β-galactosidase chimerism. The desired chimeric genotype B6 $Apc^{Min/+}$ $Mom1^{R/R}$ ↔ B6 $Apc^{Min/+}$ *ROSA26*/+ $Mom1^{R/R}$ was found at the expected frequency of 1/8.

Staining and Serial Sectioning Protocol. Whole mounts of the intestines were prepared and stained with X-Gal (United States Biological, Swampscott, MA; see *Supporting Methods*, which is published as supporting information on the PNAS web site). Sections were then postfixed in 10% formalin overnight and stored in 70% ethanol. The full intestinal tract was photographed and tumors were excised. All adenomas were embedded in paraffin, serially sectioned *in toto*, and arrayed as two 5-μm sections per slide. Every seventh slide was counterstained with hematoxylin and eosin. When a more complete analysis was required, an additional slide was counterstained with nuclear fast red. Immunohistochemistry for Apc antibody 3122 was performed as described (7), with the exception of the fixation step (see *Supporting Methods*). With experience, staining for Apc is evident in X-Gal-stained tissue.

Statistical Evaluation of the Random Collision Hypothesis. We investigated whether the polyclonality evident in a heterotypic tumor composed of both blue and white neoplastic lineages is a consequence of independent random initiation events occurring in sufficiently close proximity to result in a neoplasm scored as a single tumor (the random collision hypothesis). We tested this hypothesis by comparing the observed number of heterotypic tumors in a mouse with this quantity's posterior predictive distribution (12). The method was fully developed by Newton (M.A.N., unpublished work). Briefly, the method considers that multiple initiation events are distributed independently and uniformly at random throughout the 2D surface of the small intestine in each mouse. Monoclonal tumors would emerge from initiated clones that lie more than a distance δ from any other initiated clone. Likewise, biclonal tumors would emerge from the passive interaction between two initiated clones lying less than a distance δ from one another and more than that distance from any other initiated clones, and triclonal tumors would emerge from the interaction of three such clones. Higher-level collisions were ignored in this approximation. Tumor size measurements indicated conservatively that two tumors will be called distinct if $\delta \geq 1.5$ mm. The formulae of Armitage (13) indicate the approximate expected numbers of monoclonal, biclonal, and triclonal tumors under random collision. Random geometric graph theory (14) justifies the Poisson distribution of the tumor counts. A random-effects formulation unified the parameters of the different mice and was the basis of a Bayesian analysis to simulate the posterior predictive distribution of heterotypic tumor counts in each mouse. In this posterior simulation, the heterotypic counts are binomial-sized subsets of the numbers of biclonal and triclonal tumors. Clones are assigned types independently, according to a Bernoulli distribution. The predictive P value is the probability, under completely random collision, that an animal presenting a certain total number of tumors will also present a heterotypic tumor frequency as large as or larger than that observed.

Chimeric Patch Analysis. Digitized images revealing the chimeric patch structure of the intestinal wall adjacent to tumors were derived from X-Gal-stained whole-mount normal tissue for all unambiguously phenotyped tumors in three of the informative chimeric mice. The tissue was photographed from the serosal side so that the patch structure was not obscured by villi. Basic image processing techniques were used to form binary (blue/white) pixel images, which were processed further to measure the statistical properties of the chimeric patch structure. Distance maps show for each pixel p in a binary image the distance $d(p)$ that is the shortest distance from p to pixels of the opposite color. In addition to highlighting boundary regions typical of the loci of heterotypic tumors, these distances were useful in calculations to estimate the spatial extent of interaction among clones in polyclonal tumors. For a given image, let $F(r)$ denote the cumulative proportion of distances $d(p)$ that are no greater than r. It follows that $F(r)$ is also the probability that a disk of radius r, centered randomly on a pixel within the image lattice, will be heterotypic in that it covers both blue and white pixels. Similarly, the complement $1\text{-}F(r)$ is the probability that a randomly placed disk of radius r will be homotypic white or homotypic blue. These probabilities formed the basis of a likelihood calculation to estimate the possible spatial extent of interaction among clones of a polyclonal tumor. If polyclonality entails very short-range interactions (i.e., a small disk in the model), then the observed heterotypic fraction will be low. Conversely, longer-range interactions yield higher heterotypic fractions. In this simple disk model, the number of heterotypic tumors is a binomial random variable with success probability $\theta F(r)$, where θ is the fraction of polyclonal tumors. For $F(r)$ we used the average distribution over all available images; image-specific Fs did not improve the estimation.

As an alternative to interactions within a disk, a two-point interaction model was considered in which the number of heterotypic tumors is again binomial but in which the success probability is $\theta G(r)$, where $G(r)$ is the proportion of pixel pairs r units apart that are of opposite color; a tumor formed solely by the interaction of exactly two clones originating r units apart would be heterotypic with this probability.

Crypt Reconstruction. X-Gal-stained images reveal the chimeric patch structure but sometimes fail to display the underlying crypt layout. Instead, photographic data from a nonchimeric mouse expressing the crypt-specific *ROSA11* transgene (15) show the expected crypt patterning, variable spacing in a roughly hexagonal layout. Reconstructing the crypt layout within the chimeric patch images provided useful information such as the fraction of crypts at chimeric boundaries and the fraction of neighboring crypt pairs that were heterotypic. We applied techniques from Bayesian image analysis (16) to derive crypt reconstructions for a subset of images. The dimension of each chimeric patch image dictated the expected number N of crypts presumed to reside in that region of the intestinal surface. Unknown crypt centers $c = \{c_i: i = 1, 2, \ldots, N\}$ were viewed as points of a spatial point process having probability density $\pi(c)$, which we sampled by using the Metropolis algorithm to yield a single reconstruction $\hat{c}$ obtained after 2×10^6 single-crypt Metropolis moves from a

Table 1. Summary of mouse and tumor phenotypes

Mouse ID	% blue intestinal tissue	Count of small intestinal tumors				
		Total	Heterotypic	Homotypic blue	Homotypic white	Ambiguous phenotype
100	20	19	5	5	6	3
122	85	24	3	13	6	2
154	20	9	2	2	5	0
209	60	19	3	2	10	4
225	30	24	2	0	21	1
237	50	9	2	2	3	2
244	40	8	5	0	3	0
Total		112	22	24	54	12

square lattice initial state (17). The form $\pi(c) \propto \pi_0(c)L(c)$ ensured that $\hat{c}$ would exhibit roughly hexagonal patterning and also that the pixels representing a circular crypt i, centered at c_i, would be homotypic with high probability. We used a pair-potential Gibbs distribution wherein each pair of crypts d units apart contributes a factor $h(d)$ to $\pi_0(c)$. We set $h(d) = 0$ if $d \leq 4$ pixels, $h(d) = 1$ if $d \leq 5$ pixels, and otherwise $h(d) = \exp\{2(d - 5)\}$ following a proposal of Ripley (18). These parameters were derived from the observed layout of 283 crypt centers in the *ROSA11* image data using the method of maximum pseudolikelihood (19). The likelihood factor $L(c)$ scored crypt layout c highly if the induced crypts were homotypic in the chimeric patch image. Specifically, we took $w(i)$ and $b(i)$ equal to the numbers of white and blue pixels, respectively, in a crypt-sized circle centered at c_i, and we took W and B equal to the numbers of white and blue pixels in the intercryptal spacings. With p equal to the overall proportion of blue pixels, and with $\varepsilon = 0.02$ a small impurity rate, the chimeric patch likelihood was:

$$L(c) = \left\{ \prod_{i=1}^{N} p\varepsilon^{w(i)}(1-\varepsilon)^{b(i)} + (1-p)\varepsilon^{b(i)}(1-\varepsilon)^{w(i)} \right\} \{p^B(1-p)^W\}.$$

The rationale was that image pixels were partitioned into those close to crypt centers c_i and others, in intercryptal space, that could be simply treated as independent and identically distributed Bernoulli trials. Conceptually, crypt i realized a Bernoulli trial to be either blue or white, and then the nearby pixels retained this color except for an ε rate of impurity. Reconstructions sampled from the posterior distribution were subjected to Delaunay triangulation to identify a crypt neighborhood system (20). All statistical computations were done by using the R system (www.r-project.org).

Results

Characterization of Chimeras and Patch Patterns Generated. In this study, we have introduced the *Mom1*^{R} resistance allele in the homozygous form to reduce the intestinal tumor multiplicity in the B6 background effectively from 130 ± 35 to 16 ± 7 (a factor of 8). In addition, all animals in the study were dissected between 60 and 72 days, minimizing tumor size to ≤3 mm in maximum diameter. Together, these changes enable a very strong test of the random collision hypothesis for the development of polyclonal adenomas.

Whole-mount intestinal preparations of animals uniformly carrying the *Min* allele and chimeric for *ROSA26* were analyzed. Five of seven chimeras were found to carry white, blue, and heterotypic tumors when stained with X-Gal. The other two chimeras that overtly showed only white and heterotypic tumors were also included. In this study, a broad spectrum of chimerism between the *ROSA26* and WT lineages was observed. Whole-mount examination of intestinal tissue revealed ratios of white to blue tissue ranging from 20% to 85% (Table 1). We explicitly documented the sizes and contours of intestinal patches to develop an analysis of clonal interaction.

Histological Examination and Immunohistochemical Analysis of Adenomas. Intestinal tumors were initially identified by examining X-Gal-stained whole-mount sections under a dissecting microscope. All adenomas were photographed, excised, and serially sectioned through the entire tumor (see *Materials and Methods*). In contrast to previous work, the fixation and staining protocols (see *Supporting Methods*) permitted much deeper penetration of X-Gal staining within adenomas (Fig. 1). Tissue within tumors was assessed for neoplastic transformation by inspection of stained slides (see *Materials and Methods*) based on histopathologic characteristics such as architectural distortion, nuclear atypia, and increased nuclear/cytoplasmic ratio. In some instances, X-Gal-stained sections were counterstained with nuclear fast red to clarify the distribution of X-Gal staining. We frequently observed adenomas in which histologically normal crypts seemed to lie within the tumor. We examined two heterotypic and two white adenomas by immunohistochemistry with the polyclonal Apc antibody 3122. Within the histologically unambiguous heterotypic adenomas, both the blue and the white tumor tissue were found to be negative for Apc. Our results were consistent with the report of Merritt *et al.* (7) that all lineages within polyclonal adenomas lose Apc expression. In some tumors composed of both X-Gal-positive and -negative tissue components, it was uncertain based on histologic appearance alone whether both tissue types were transformed. Twelve such ambiguous tumors were observed (Table 1).

Analysis of Tumor Multiplicity. In total, 112 adenomas of the small intestine were identified from the seven chimeric animals having the desired genotype (B6 *Apc*$^{Min/+}$ *Mom1*$^{R/R}$ ↔ B6 *Apc*$^{Min/+}$ *Mom1*$^{R/R}$ *ROSA26*/+). Of these 112 adenomas, 54 appeared to be homotypic white, 24 homotypic blue, 22 heterotypic, and 12

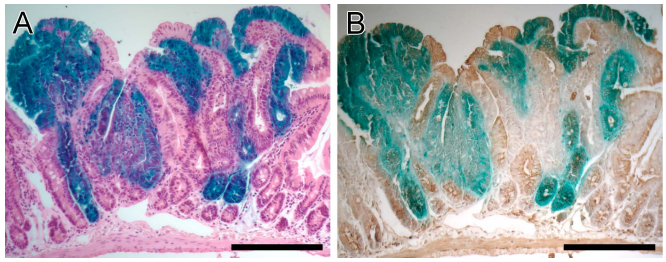

Fig. 1. Histological sections of a heterotypic small intestinal adenoma stained with X-Gal (blue). (*A*) Section also stained with hematoxylin and eosin. (*B*) An adjacent section also stained with Apc antibody 3122 (brown) and lightly counterstained with hematoxylin. (Bars: 200 μm.)

a distance r. Qualitatively this model mirrors the previous disk model, although it gives limited information on the upper bound to the range of clonal interaction (data not shown).

Analysis of Clonal Interaction by Crypt Reconstruction. The Metropolis sampling method was used to simulate the crypt arrangement in 17 representative images from three of the seven chimeric mice (images adjacent to two blue, two white, and two heterotypic tumors from animals 100, 122, and 154, except just one blue tumor in 154). Delaunay triangulation of the reconstructed crypt centers provided a neighborhood system that, as expected, showed a roughly hexagonal pattern. Fig. 4 *A* and *B* shows the triangulated reconstruction for one image. The neighborhood system surrounding a typical crypt includes first-, second-, and higher-order neighbors (Fig. 4*C*). On average over all analyzed images, we computed the number of *n*th-order neighbors (Fig. 4*D*) and the proportion of *n*th-order neighbors that are isotypic to the centering crypt (Fig. 4*E*). Fig. 4*F* shows the heterotypic fraction under various scenarios of polyclonal tumor formation. For example, if, on average, 50% of all first- and second-order neighboring crypts were to participate in a polyclonal tumor with an initiated crypt, then the probability that this tumor would be heterotypic is ≈60%. This calculation revealed that the observed heterotypic fraction (22%) is easily explained by intercryptal interactions spanning one or two crypt diameters.

The tumor distribution throughout the intestinal tract is significantly different for heterotypic tumors compared with homotypic tumors. Although Min tumor multiplicity is elevated in the distal region of the small intestine (9), the proportion of heterotypic tumors was higher in the proximal region. (Overall, 11 heterotypic and 13 homotypic tumors in the proximal half versus 11 heterotypic and 65 homotypic tumors in the distal half; $P = 0.001$, χ^2 test.) An ANOVA indicated no significant difference in patch structure between the proximal and distal regions of the small intestine that could explain these data. In addition, no significant difference in tumor size could be documented between homotypic and heterotypic tumors when compared segment by segment, although the statistical power of this test was limited by the low tumor multiplicity. These findings also weigh against the random collision hypothesis.

Discussion

In this study we have sought first to test rigorously the random collision hypothesis for the formation of polyclonal familial intestinal adenomas. The random collision hypothesis being tested states that every crypt in the intestine acts independently with an equal probability of generating an adenoma. Several lines of evidence against this hypothesis have emerged.

Chimeric mice were established in which the tumor multiplicity was decreased to 16 ± 7 over the entire intestinal tract, a factor of 8 lower than in our previous study (7). This reduction in multiplicity, accompanied by a reduction in tumor size, permitted an explicit calculation of the expected probability distribution for the number of heterotypic tumors. The observed numbers were far higher than predicted by the random collision hypothesis ($P < 0.01$).

A modification of the random collision hypothesis considers that the intestinal tract is regionally heterogeneous in tumor susceptibility (21). Again, our findings weigh against this regionally restricted collision hypothesis: heterotypic tumors were observed more frequently in the proximal region of the small intestine, where tumor multiplicity is lower than in the distal region (9).

Ruling out both the random and the regionally restricted collision hypotheses, we have next analyzed clonal interaction models by methods of spatial statistics. Through several different statistical analyses, we connected the chimeric patch structure to

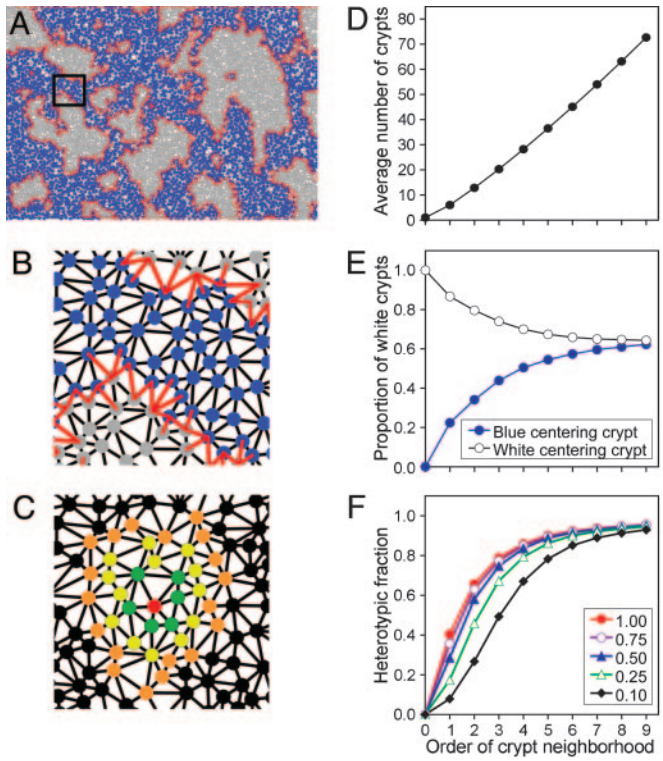

Fig. 4. Crypt reconstruction and analysis. (*A*) Crypt reconstruction. The arrangement of 5,462 crypts presumed to reside on the intestinal surface imaged in Fig. 2*B* is reconstructed by Metropolis chain simulation of a distribution over all possible crypt arrangements. This posterior distribution is informed by the known crypt arrangement from a *ROSA11* mouse (expanded version of Fig. 3*B*), which constitutes a prior distribution of arrangements, and by the binary image (Fig. 2*B*), according to techniques from Bayesian image reconstruction (see *Materials and Methods*). The techniques give higher likelihood to arrangements in which all of the pixels within a crypt have the same color. Crypt centers from one realization of the posterior distribution are plotted; crypts are colored according to a majority rule of contained pixels. Crypt neighbors are determined by Delaunay triangulation, and the connecting edges are drawn in red if the adjacent crypts are heterotypic. This reconstruction contains 16,902 neighboring crypt pairs, 14% of which are heterotypic. If, for example, polyclonal tumors form by the interaction of two neighboring crypts in a chimeric intestinal surface like Fig. 2*A*, then we estimate that 14% of such tumors would be heterotypic. This is the crypt pair phenotype index (2). (*B*) Crypt reconstruction detail. Shown is a higher magnification of the area marked in *A*. (*C*) Crypt neighborhood system. One crypt from *B* is highlighted in red and its neighbors of various orders are indicated by different colors. For instance, this crypt has 6 nearest neighbors (green) and 13 second-order neighbors (yellow). (*D*) Crypt neighborhood statistics. Crypt reconstructions as in *A* were obtained for 17 representative images, and neighborhoods were identified for all crypts. Plotted for various neighborhood orders is the average number of neighbors for each crypt. To avoid boundary problems, the average is computed over all interior crypts in all images, where a crypt is interior if it resides in the middle 80% of the image in both coordinates. On average, crypts are within a few steps of many other crypts. (*E*) Heterotypic crypt neighborhoods. Averaging as in *D*, we compute for each white crypt the average proportion of white crypts in its *n*th-order neighborhood (white circles) and for each blue crypt the average proportion of white crypts in its *n*th order neighborhood (blue circles). White crypts tend to lie near white crypts, and similarly for blue, but the patch sizes are such that two crypts seven or eight steps apart have independent colors. (*F*) Heterotypic tumor fraction. Averaging as in *D* and *E* we compute the probability Ψ that a tumor is heterotypic, using various levels of crypt interaction. Shown in red is Ψ when a tumor is formed from all crypts within an *n*th order neighborhood of some initiated crypt. Less than complete involvement is indicated by the other curves. For instance, the blue curve shows Ψ when each curve within an *n*th-order neighborhood of an initiated crypt tosses a fair coin to decide whether or not to participate in the tumor. Importantly, the observed heterotypic fraction (22%) can be explained by intercryptal interactions between first- or second-order neighbors for a wide range of participation rates.

the heterotypic counts and thus measured the likely spatial extent over which clones interact in the establishment or growth of tumors. The disk model calculations approximate this interaction by supposing that a polyclonal tumor is formed through the participation of crypts that lie within a disk placed uniformly on the intestinal surface. With a relatively high polyclonal fraction, very small disks can explain the observed heterotypic fraction.

More detailed inferences were possible when the crypt pattern, from a *ROSA11* mouse, was superimposed on the chimeric pattern (Fig. 4). This analysis demonstrates that, even if an initiated crypt interacts with only a small fraction of its nearest neighboring crypts, the predicted heterotypic fraction will meet the observed 22%.

Our studies of familial intestinal adenomagenesis indicate the importance, if not the necessity, of short-range clonal interactions. These interactions can either involve groups of nearest-neighbor monoclonal crypts or else distinct clones within the single polyclonal crypts that are common in neonates before crypt purification (22). Our analysis of chimeric patch patterns is consistent with a proportion of polyclonal adenomas ranging from the overtly heterotypic incidence of 22% to 100%. Although these chimeras have permitted spatial resolution superior to that of X-inactivation mosaics in the human (4), still higher resolution will be needed to refine this estimate, to determine whether polyclonality is a necessary condition for adenomagenesis, and to ascertain whether polyclonal single crypts are important progenitors.

The inference of short-range clonal interactions in familial intestinal neoplasia seems inconsistent with the observation that each participating clone has lost the expression of the WT Apc allele (ref. 7 and this study). Hits in *Apc/APC* occur early during tumorigenesis in the mammalian intestine (14, 23). Haigis and Dove (24) demonstrated that the WT allele of *Apc* is lost by somatic recombination during intestinal tumorigenesis in B6 Min mice. How can multiple loss-of-heterozygosity events arise simultaneously, either in a very small neighborhood or within a single polyclonal crypt? One possibility is microheterogeneity in tumor susceptibility. Regions of stroma may promote loss of heterozygosity in the associated epithelium. Alternatively, loss of Apc/APC in one epithelial clone may induce the expression of growth factors that affect mitotic rates in neighboring clones. The normal intestinal epithelium adjacent to tumors is often hyperplastic (25). Thus, the multiple hits in *Apc/APC* that occur in polyclonal familial adenomas in the mammalian intestine may not be independent of one another.

This microheterogeneity would give rise to epithelial neoplasms that are focal even if not clonal. If several clones within a focus simply share a neighborhood or niche, but do not exchange biologically relevant signals, this focal interaction would have a passive character. On the other side, an apparently clonal early neoplasm may involve interaction between progenitors. For example, crypt fission is frequent in the colon of familial adenomatous polyposis patients (26). If initiated sister crypts formed by fission were to cooperate in adenomagenesis, the emergent tumors would be monotypic for a lineage marker.

Clearly the analysis of clonal interactions in the establishment, growth, and progression of intestinal neoplasms (familial, sporadic, and carcinogen-induced) deserves the continuing attention of cancer biologists and statisticians.

We thank the McArdle Histotechnology Group, in particular Jane Weeks and Harlene Edwards, for outstanding assistance. Our manuscript has received careful critical review from Norman Drinkwater, Richard Johnson, Cheri Pasch, and Alexandra Shedlovsky. Our research was supported by National Cancer Institute Grants R37CA63677, U01CA84227, K08CA84146, and R01CA64364. This is publication no. 3622 from the Laboratory of Genetics, University of Wisconsin.

1. Ponder, B. A. J. & Wilkinson, M. M. (1986) *J. Natl. Cancer Inst.* **77,** 967–973.
2. Griffiths, D. F. R., Williams, D., Williams, G. T. & Williams, E. D. (1989) *Br. J. Cancer* **59,** 385–387.
3. Fearon, E. R., Hamilton, S. R. & Vogelstein, B. (1987) *Science* **238,** 193–197.
4. Novelli, M., Cossu, A., Oukrif, D., Quaglia, A., Lakhani, S., Poulsom, R., Sasieni, P., Carta, P., Contini, M., Pasca, A., *et al.* (2003) *Proc. Natl. Acad. Sci. USA* **100,** 3311–3314.
5. Novelli, M. R., Williamson, J. A., Tomlinson, I. P. M., Elia, G., Hodgson, S. V., Talbot, I. C., Bodmer, W. F. & Wright, N. A. (1996) *Science* **272,** 1187–1190.
6. Newton, M. A. (2005) *On Estimating the Polyclonal Fraction in Lineage-Marker Studies of Tumor Origin*, University of Wisconsin, Department of Statistics, Technical Report 1099 (University of Wisconsin, Madison).
7. Merritt, A. J., Gould, K. A. & Dove, W. F. (1997) *Proc. Natl. Acad. Sci. USA* **94,** 13927–13931.
8. Gurdon, J. B., Lemaire, P. & Kato, K. (1993) *Cell* **75,** 831–834.
9. Haigis, K. M., Hoff, P. D., White, A., Shoemaker, A. R., Halberg, R. B. & Dove, W. F. (2004) *Proc. Natl. Acad. Sci. USA* **101,** 9769–9773.
10. Gould, K. A., Luongo, C., Moser, A. R., McNeley, M. K., Borenstein, N., Shedlovsky, A., Dove, W. F., Hong, K., Dietrich, W. F. & Lander, E. S. (1996) *Genetics* **144,** 1777–1785.
11. Cormier, R. T., Bilger, A., Lillich, A. J., Halberg, R. B., Hong, K. H., Gould, K. A., Borenstein, N., Lander, E. S. & Dove, W. F. (2000) *Oncogene* **19,** 3182–3192.
12. Gelman, A., Carlin, J. B., Stern, H. S. & Rubin, D. B. (2004) *Bayesian Data Analysis* (Chapman & Hall, Boca Raton, FL).
13. Armitage, P. (1949) *Biometrika* **36,** 257–266.
14. Penrose, M. (2003) *Random Geometric Graphs* (Oxford Univ. Press, Oxford).
15. Gould, K. A. & Dove, W. F. (1996) *Cell Growth Differ.* **7,** 1361–1368.
16. Besag, J. (1986) *J. R. Stat. Soc. B* **48,** 259–302.
17. Liu, J. S. (2001) *Monte Carlo Strategies in Scientific Computing* (Springer, New York).
18. Ripley, B. D. (1977) *J. R. Stat. Soc. B* **39,** 172–212.
19. Besag, J. (1974) *J. R. Stat. Soc. B* **36,** 192–236.
20. Lee, D. T. & Schacter, B. J. (1983) *Int. J. Comput. Information Sci.* **9,** 219–242.
21. Dove, W. F., Cormier, R. T., Gould, K. A., Halberg, R. B., Merritt, A. J., Newton, M. A. & Shoemaker, A. R. (1998) *Philos. Trans. R. Soc. London B* **353,** 915–923.
22. Schmidt, G. H., Winton, D. J. & Ponder, B. A. J. (1988) *Development (Cambridge, U.K.)* **103,** 785–790.
23. Levy, D. B., Smith, K. J., Beazer-Barclay, Y., Hamilton, S. R., Vogelstein, B. & Kinzler, K. W. (1994) *Cancer Res.* **54,** 5953–5958.
24. Haigis, K. M. & Dove, W. F. (2003) *Nat. Genet.* **33,** 33–39.
25. Bjerknes, M. & Cheng, H. (1999) *Am. J. Pathol.* **154,** 1831–1834.
26. Wasan, H. S., Park, H. S., Liu, K. C., Mandir, N. K., Winnett, A., Sasieni, P., Bodmer, W. F., Goodlad, R. A. & Wright, N. A. (1998) *J. Pathol.* **185,** 246–255.